Journal Name

ARTICLE TYPE

Cite this: DOI: 10.1039/xxxxxxxxxx

Capturing the interplay between spin-orbit coupling and non-Condon effects on the photoabsorption spectra of Ru and Os dyes

Theo Keane,[*a,b] Thomas W. Rees,[c] Etienne Baranoff,[c] and Basile F. E. Curchod[*d]

Received Date
Accepted Date

DOI: 10.1039/xxxxxxxxxx

www.rsc.org/journalname

In this work, we investigate the factors influencing the shape of the low-energy tail of the absorption spectrum of a homoleptic biscyclometalated ruthenium complex with terdentate ligands [Rees *et al., Inorganic Chemistry*, 2017, **56**, 9903] by combining an advanced theoretical strategy and the synthesis of an analogous Osmium complex. The theoretical protocol merges relativistic linear-response time-dependent density functional theory and the nuclear ensemble approach, permitting to shed light on the influence of spin-orbit coupling and non-Condon effects on the theoretical absorption spectra of these rather large metal complexes.

Introduction

Reproducing the absorption of visible light by metal complexes using computational methods is paramount in the process of studying and designing molecules with specific properties for applications such as solar cells, sensors, and organic light emitting diodes. At first glance, this task may appear simple. However, several factors complicate the calculations and are likely to hamper a satisfactory reproduction of the different absorption bands – e.g. the influence of a solvent, the breakdown of the Condon approximation, or the presence of relativistic effects – although their addition to an *ab initio* model should ultimately provide a more comprehensive and accurate description of the processes at the origin of the absorption properties of a dye. A lot of effort has recently been devoted to include the role of the environment on the light absorption capabilities of a given molecule (see e.g. Refs. 1–3). Therefore in the following, we will focus on the role of non-Condon and relativistic effects and propose a brief survey of selected strategies to address the underlying challenges.

The simplest strategy to reproduce an absorption spectrum for a given molecule is to first locate the minimum (possibly minima) on the ground state potential energy surface. At the nuclear configuration corresponding to this equilibrium geometry (black dot on the upper panel of Fig. 1a), excited-state electronic structure methods can be employed to determine *vertical transition energies*, *i.e.*, differences in electronic energies between a subset of excited electronic state and the ground state, at the equilibrium geometry (vertical arrows in Fig. 1a), as well as the corresponding transition probabilities. As information about the excited state is only known at the equilibrium geometry, plotting these vertical transitions gives rise to a "stick plot", which can be further Gaussian- or Lorentzian-broadened to better mimic the experiment (right panel of Fig. 1a). If more than one conformation is thermally populated, a similar treatment can be applied at additional minima, and the final spectrum becomes the weighted sum of the spectra at each minimum. Whilst simple, this single-point (SP) strategy already offers a powerful tool to investigate the character of the different excited states and to assign transitions in an experimental spectra. However, the classical approximation for the nuclei encoded in the SP strategy does not allow for the description of vibronic progressions and leads also to a neglect of non-Condon effects (*i.e.*, the fact that electronic transition dipole moments are not constant with respect to a change in nuclear geometry.

An important component of absorption spectra that is missed with the SP strategy is the vibrational component associated to electronic transitions, caused by overlaps between the ground and the excited electronic states vibrational wavefunctions. One of the most accurate ways of recovering such vibronic features requires quantum dynamics simulations.[4] Unfortunately, the computational cost associated with this strategy beyond ten atoms hampers its general applicability, and the quantum effects related to the nuclear degrees of freedom have to be approximated. Re-

[a] *Department of Chemistry, University of Sheffield, Brook Hill, Sheffield, S3 7HF, UK; E-mail: t.keane@shef.ac.uk*
[b] *School of Natural and Environmental Sciences, Newcastle University, Newcastle upon Tyne, NE1 7RU, UK.*
[c] *School of Chemistry, University of Birmingham, Edgbaston, Birmingham B15 2TT, UK.*
[d] *Department of Chemistry, Durham University, South Road, Durham DH1 3LE, UK; E-mail: basile.f.curchod@durham.ac.uk*

† Electronic Supplementary Information (ESI) available. See DOI: 10.1039/b000000x/

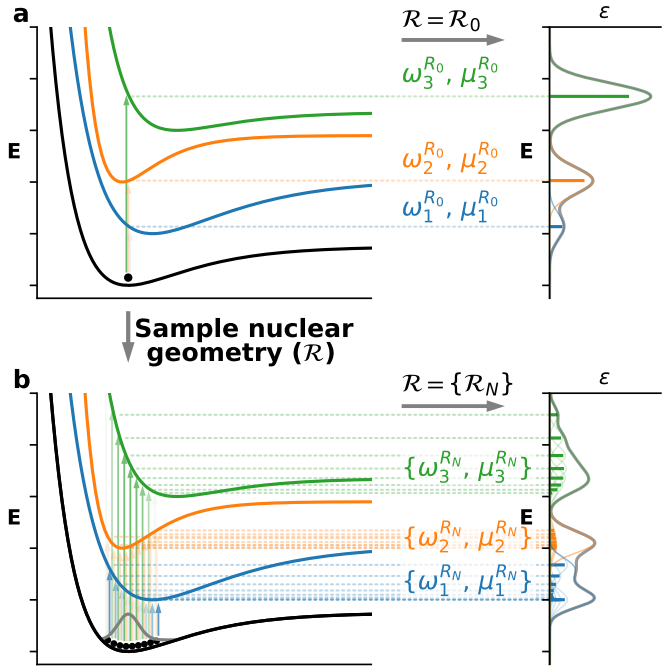

Fig. 1 Schematic representation of two different strategies for the simulation of absorption spectra. a) Theoretical absorption spectra based solely on a single nuclear configuration – the electronic ground state geometry, $\mathbf{R}_0$ – and its associated transition energies ($\omega_I^{\mathbf{R}_0}$) and transition dipole moments ($\mu_I^{\mathbf{R}_0}$) to the excited states I. b) The Nuclear Ensemble Approach approximates the width and intensity of a vibronic band by sampling a number of nuclear configurations in the ground state from an approximate quantum distribution. For each nuclear geometry $\mathbf{R}_N$ of the ensemble, one calculates the transition energies $\omega_I^{\mathbf{R}_N}$ and transition dipole moments $\mu_I^{\mathbf{R}_N}$), and produces an absorption spectrum. The final NEA absorption spectrum is produced by averaging over all spectra.

cent works have proposed the use of semiclassical dynamics for example[5].

To make the calculations more tractable, a first possible approximation is to capture the vibronic progressions of absorption spectra in a Franck-Condon picture, *i.e.*, by calculating Franck-Condon factors. Furthermore, if needed, Franck-Condon factors can be augmented with Herzberg-Teller corrections, that account for non-Condon effects (see e.g. Ref. 6). The calculation of Franck-Condon factors requires the determination of nuclear wavefunctions for both the ground and the excited electronic state of interest. For medium- to large-size molecules (beyond 10 atoms), this often implies the use of an harmonic approximation.[6–9]

Another strategy, called the nuclear-ensemble approach (NEA), proposes to reproduce, approximately, the width of a vibronic band without the explicit calculation of nuclear wavefunctions.[10–12] The idea of the NEA is to sample nuclear configurations in the ground electronic state (points in Fig. 1b), and to compute vertical transition energies and probabilities for each of them. A small phenomenological broadening is applied to each transition energy, and a photoabsorption cross-section can be calculated by averaging over all the sampled configurations[10] (Fig. 1b). A theoretical justification for the NEA can be found in Ref. 11. This strategy can be applied to molecular systems in their full configuration space, as the NEA only requires the sampling of nuclear configurations on the ground state and does not need information on the excited states, besides transition energies. Vibronic progressions are not accounted for as a result of the underlying approximations, but the NEA offers a straightforward way to approximate the width and the intensity of absorption spectra, including non-Condon effects (dark transitions can gain intensity as a result of the sampling of nuclear geometries). A question remains: how should we sample the electronic ground state (the dots in Fig. 1b)? One possibility is to use molecular dynamics to generate a thermal ensemble[13] or more advanced dynamics strategies to recover the effect of zero-point energy in the sampling (for example quantum thermostat[14,15]). A simpler strategy consists in considering that the molecule is mostly harmonic and sampling nuclear configurations from a Wigner distribution for a set of uncoupled harmonic oscillators (the normal modes of the molecule considered).[16] This last sampling assumes that the molecule is in its ground vibrational level (zero-point level), and generates an approximate quantum sampling.[13] This strategy has only been sparsely employed in the calculation of absorption spectra of metal complexes (see *e.g.* Refs[17–19]).

Up to this point, we have considered that reliable excitation energies and oscillator strengths can be obtained for the molecule of interest. While there are a number of different electronic structure methods that can be used for calculating excitation energies[20], our interest in (large) metal complexes forces us to focus on linear-response time-dependent density functional theory (LR-TDDFT).[21–24] Also, the electronic states of molecules containing late transition metal complexes can be strongly influenced by the presence of relativistic effects, in particular spin-orbit coupling (SOC), and recent developments allowed to include spin-orbit coupling in LR-TDDFT.[25–27] Such strategy was used to successfully compute SOC effects in metal complexes[28–32] using the SP approach described above.

In this work, we propose to combine some of the strategies described above to shed light on specific features of the absorption spectrum of a recently reported[33] homoleptic biscyclometalated ruthenium complex with terdentate ligands, **1-Ru** (Fig. 2). **1-Ru** exhibits an absorption spectrum with a low energy tail at around 700 nm (see upper panel of Fig. 3), and previous calculations based on a SP strategy and LR-TDDFT (without the inclusion of SOC) suggested that this low-energy tail should be dominated by singlet metal-to-ligand charge transfer (^{1}MLCT) transitions[33]. We propose here a study of **1-Ru** combining the Nuclear Ensemble Approach with relativistic LR-TDDFT, allowing us to decipher the role played by SOC and non-Condon effects in the low-lying transitions of **1-Ru**. In addition, an analogue of **1-Ru**, **1-Os** (Fig. 2) – differing from **1-Ru** only by a Ru-to-Os substitution – was synthesised to further probe the importance of SOC in the low-lying electronic states of this family of metal complexes, offering an additional test for the theoretical protocol proposed here.

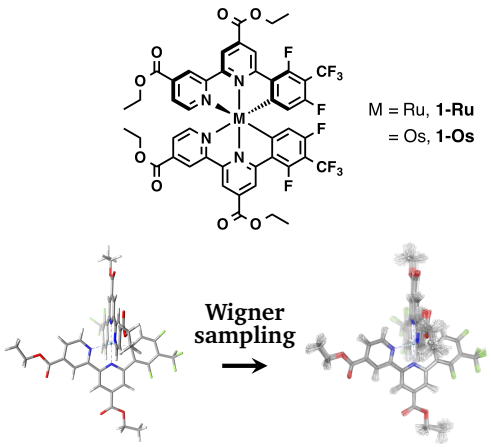

Fig. 2 Structure of complex **1** (top); Optimised geometry of **1-Os** (left) and geometries sampled from the approximate Wigner distribution (right).

Methods

Geometry optimisation and frequency calculations were performed using the software package Gaussian 09[34] using density functional theory (DFT) with the PBE0 functional[35] and the dhf-TZVP and def2-TZVP(-f) basis sets for the metals and other atoms, respectively.[36–38] Grimme's dispersion correction with Becke-Johnson damping, D3(BJ), was applied,[39–41] and solvent effects (dichloromethane) were included implicitly using a CPCM.[42] A Wigner function for uncoupled harmonic oscillators was constructed from the DFT ground-state geometry and corresponding harmonic frequencies using Newton-X[43], from which 30 nuclear geometries were randomly sampled (see lower panel of Fig. 2). The cost of the calculations, in particular with the inclusion of relativistic effects, limited the number of sampled configurations.

We note that hybrid functionals like PBE0 have been found to be a good compromise to describe the different types of electronic-state characters found in metal complexes of the types studied in this work (see for example Refs.[44–48]). In particular, MLCT transitions in these complexes do not suffer particularly from the charge-transfer problem inherent to the use of LR-TDDFT in its adiabatic representation[24]. Other types of metal complexes, however, may require a long-range corrected functional for an adequate description of their MLCT transitions, as reported for example in Refs.[49,50]. It is important to emphasize, though, that while the methodology introduced here proposes to improve the description of absorption spectra by including physical effects like spin-orbit coupling and non-Condon phenomena, its overall result strongly relies on the quality of the approximations used to calculate the electronic structure of the molecule. In the following, we use PBE0 as a compromise for the description of the different electronic states. Nevertheless, the methodology could be employed with any electronic-structure methods that can incorporate spin-orbit coupling.

One component (1C) scalar relativistic and Kramers restricted two-component (2C) relativistic DFT calculations were performed using the exact two-component (X2C) Hamiltonian, as implemented in the Turbomole software package.[51–53] We note that the 1C calculations include only scalar relativistic corrections, thus singlets and triplets remain unmixed and spin selection rules apply. In contrast, the 2C calculations include all relativistic effects, thus singlet and triplet states are able to mix *via* spin-orbit coupling, and so formally spin-forbidden transitions are allowed in 2C calculations. The PBE0 functional was used in combination with the all electron x2c-SV(P)all and x2c-SV(P)all-2c basis sets,[54] specifically designed for use with the 1C-X2C and 2C-X2C Hamiltonians, respectively. Dichloromethane solvent effects were included implicitly using COSMO.[42] Relativistic 1C and 2C LR-TDDFT calculations were performed within the Tamm-Dancoff approximation,[27,55] which further offers a more accurate description of triplet transition energies.[56]

Excited-state wavefunction analysis[57] of the 1C calculations was conducted using the TheoDORE software package.[58] Wavefunction analysis is used to decompose excitations in terms of their charge-transfer characteristics, Ω_i, where i = Metal-to-Ligand Charge Transfer (MLCT), Ligand-to-Metal Charge Transfer (LMCT), Ligand-to-Ligand Charge Transfer (LLCT), Ligand-Centred (LC) and Metal-Centred (MC) transitions. More in-depth analysis of the excitations within the visible region, in the form of electron-hole correlation plots,[59] is provided in the ESI.

We refer to absorption spectra calculated only at the optimised ground-state geometry as "single-point" (SP) spectra, and spectra calculated using the Wigner-sampled geometries as "Wigner-sampled" (WIG) spectra. In the 1C calculations, 20 singlet and 20 triplet excited states were calculated per geometry. In the 2C calculations, 100 coupled states were calculated for the single-point spectra and 30 coupled states per geometry for the Wigner spectra.

We point out that, besides the challenge of choosing an appropriate exchange and correlation functional and basis set for the molecule of interest, additional care has to be taken when employing the NEA. In particular, the approximations for the Wigner distribution (uncoupled harmonic oscillators) is likely to break down if the molecule has strongly anharmonic modes or if an explicit description of the environment (solvent) is required. Strategies to overcome the limitation of the approximate Wigner sampling have recently been proposed for metal complexes.[18]. Fortunately, the geometric constrains of the present ligand system, combined with the weakly interacting nature of the solvent employed (dichloromethane) mean that the Wigner sampling strategy appears reasonable in the present case.

The synthesis and characterisation are available in the SI for **1-Os** and in Ref.[33] for **1-Ru**.

Results and Discussion

We start our discussion of the **1-Ru** and **1-Os** absorption spectra by comparing their scalar relativistic 1C single-point vertical transitions to experimental data (Fig. 3), along with the results of an electronic-character analysis. The similarity between the calculated scalar relativistic spectra of **1-Ru** and **1-Os** is striking, even if the character of the transitions that underpin the absorption spectra slightly differ between the two molecules. Within the visible region, **1-Ru** states appear to have a greater MLCT character

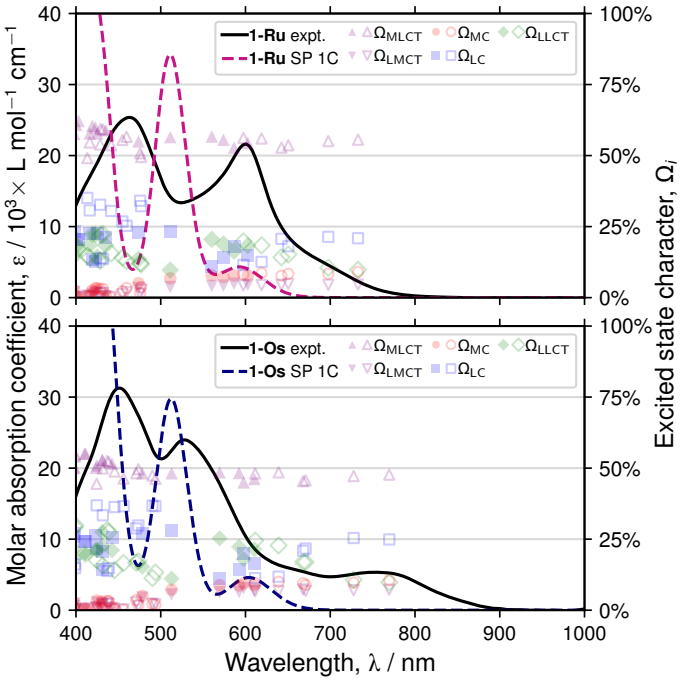

Fig. 3 Comparison of the excited-state characters between **1-Ru** (top) and **1-Os** (bottom) for single-point 1C calculations. The charge-transfer characteristics, Ω_i (as defined in the Methods section) are shown for each singlet (filled shapes) and triplet (empty shapes) excited state. Each transition is broadened with Gaussian functions (FWHM = 0.2 eV).

than **1-Os** states. At the 1C level, there are only small energetic differences between the **1-Ru** and **1-Os** singlet manifolds, and the **1-Os** triplets are slightly lower in energy than those of **1-Ru**. Overall, this suggests that the main differences in the experimental absorption spectra are related to the difference in spin-orbit coupling effects between the two complexes, as observed for various Ru and Os complexes.[31,32] For both **1-Ru** and **1-Os**, there are two prominent peaks in the visible region. The calculated peaks at ∼600 nm have contributions from $S_0 \rightarrow S_1$ and $S_0 \rightarrow S_2$, near-degenerate transitions consisting of charge-transfer onto the bipy-subunits of the NNC ligands, with notable inter-ligand character. T_1 and T_2 are of similar character to each-other, and are situated ∼0.4 eV below S_1 and S_2. On the red side of the calculated ∼600 nm peaks, there are four nearby triplets (T_3 to T_6), and two dark singlet states (S_3 and S_4) on the blue side. The calculated peaks at ∼510 nm are due to $S_0 \rightarrow S_5$, primarily MLCT onto the outer pyridine moieties. There is then a gap of ∼0.4 eV before a large density of allowed $S_0 \rightarrow S_n$ transitions.

We extend our investigation by now including the effect of spin-orbit coupling, but by still preserving a SP picture. The scalar relativistic 1C and spin-orbit coupled 2C single-point spectra of **1-Ru** and **1-Os** are compared in Figure 4. For **1-Ru**, the differences between the 1C and 2C spectra are rather small: the 2C single-point spectrum mostly differs from the 1C one by an additional, broad peak from 620 – 730 nm and a slight drop in intensity of the ∼600 nm peak. The new broad peak is located in the region of the low-lying 1C triplets and arises from sizeable SOC effects allowing for intensity borrowing effects between the low-lying singlet and triplet states of **1-Ru**. There is a small blue shift of the peak at ∼510 nm, and an increase in intensity of the features between 450 – 490 nm. Overall, the influence of spin-orbit coupling appears to be rather weak in **1-Ru**, consistent with previous investigations.[31] In contrast, the dramatic effect of spin-orbit coupling is clearly visible by comparing the 1C and 2C absorption spectra for **1-Os** (Fig. 4). The 2C calculated single-point spectrum of **1-Os** exhibits an intense, broad feature between 650 – 900 nm, commensurate with the calculated 1C triplet energies. The new feature is more intense than the slightly blue shifted feature at 540 – 650 nm. A more pronounced blue shift of the adjacent feature is observed, now located at ∼490 nm. Earlier works on different osmium complexes observed a similar blue shift of the bands in this spectral range upon inclusion of SOC (using a perturbative approach).[31,60]

The spectral changes observed when going from the scalar relativistic 1C calculations to the spin-orbit coupled 2C calculations assist in the assignment of the experimental absorption peaks in **1-Ru** and **1-Os**. The blue shift of the calculated peak in the 500 nm region of **1-Os** compared to **1-Ru** suggests that these calculated transitions correspond to the experimental peaks observed at 600 nm and 530 nm in **1-Ru** and **1-Os**, respectively. We note that LR-TDDFT/PBE0 appears to overestimate the energy of the low-lying transitions, particularly for **1-Ru**, despite their charge-transfer character. The results presented thus far corroborate the observations of earlier theoretical works[31,32] that the prominent low-energy band in cyclometalated osmium complexes is caused by SOC, while this relativistic effect appears to play a less important role in the absorption spectra of similar ruthenium complexes.

We now examine the influence of including non-Condon effects in the absorption spectra by sampling different molecular configurations from a quantum distribution in the ground state using the NEA described above, both with and without the inclusion of SOC. As such sampling results in a distribution of nuclear geometries, each with a different set of vertical transition energies and corresponding oscillator strengths (see Fig. 1), the NEA allows us to go beyond the single-point picture by explicitly including the effect of different nuclear geometries on the vertical excitation energies and transition probabilities. The Wigner-sampled spectra of **1-Ru** and **1-Os** at both scalar relativistic 1C and spin-orbit coupled 2C levels are compared in Figure 5. We note that the sampling inherent to the use of the NEA can become computationally expensive for molecules of the size of **1-Ru** and **1-Os** (in particular when SOC effects are included), and this limited our investigation to 30 configurations. For **1-Ru**, a remarkable similarity between the 1C and 2C Wigner-sampled spectra is observed. Whereas in the single-point calculations, the 2C spectrum of **1-Ru** displays additional features when compared to the 1C spectrum (see Fig. 4), in the Wigner-sampled spectra, the number and position of the features in both 1C and 2C spectra are similar, highlighting the influence of non-Condon effects recovered upon averaging over an ensemble of nuclear configurations. Both 1C and 2C Wigner-sampled spectra display a broad feature in the 600 – 800 nm region, with only small differences in intensity between the two spectra. Likewise, both spectra display a band splitting of

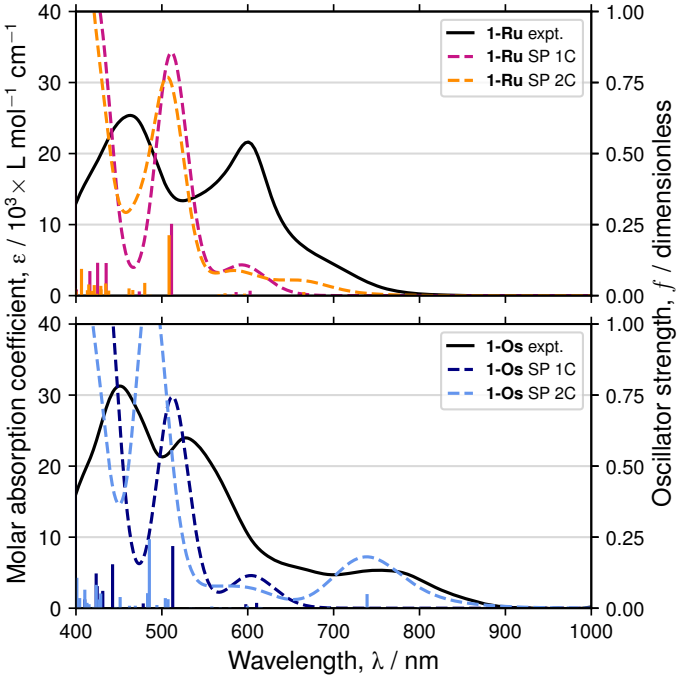

Fig. 4 Experimental Vis/NIR absorption spectra of **1-Ru** (top) and **1-Os** (bottom) compared with scalar relativistic (1C) and fully relativistic (2C) single-point spectra. Transitions are broadened with Gaussian functions (FWHM = 0.2 eV).

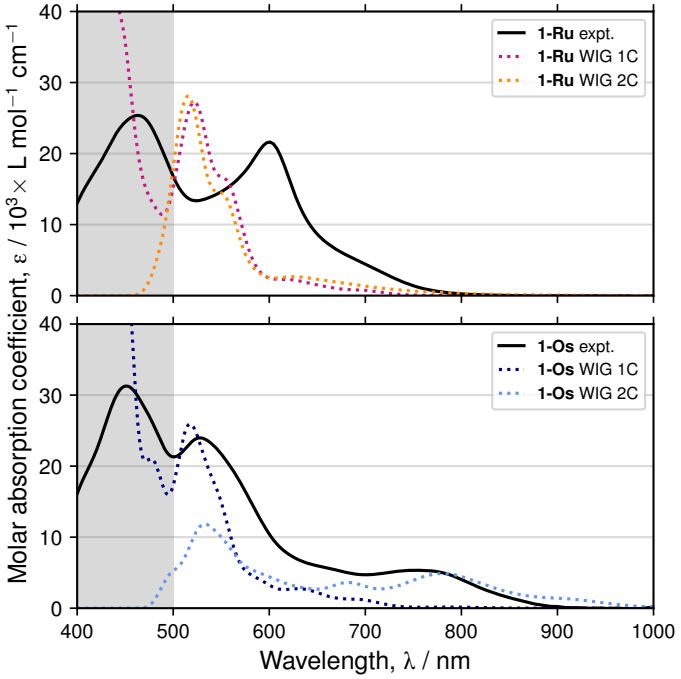

Fig. 5 Experimental Vis/NIR absorption spectra of **1-Ru** (top) and **1-Os** (bottom) compared with scalar relativistic (1C) and fully relativistic (2C) Wigner-sampled (WIG) spectra. Note that due to the high cost of 2C calculations, the 2C spectra included fewer excitations and are thus truncated at approximately 500 nm, as indicated by the grey area. Transitions are broadened with Gaussian functions (FWHM = 0.1 eV).

the central band observed at ∼510 nm in the SP spectra. This observation suggests that non-Condon effects can compete with the influence of spin-orbit coupling transitions in the overall shape of the low-energy tail of the **1-Ru** absorption spectrum. Hence, these results highlight the potential influence of nuclear configurations on the interpretation of electronic spectra of Ru complexes, but appear to confirm the assignment of the low-energy tail of the absorption spectrum as exhibiting dominantly a ^{1}MLCT character[33]. It is also interesting to note that nuclear geometry sampling does not alleviate the apparent tendency of LR-TDDFT/PBE0 to overestimate the excitation energies: the calculated spectra remain blue-shifted with respect to the experimental spectrum.

Given the strong spin-orbit coupling displayed by **1-Os** (Fig. 4), the drastic differences observed between the Wigner-sampled 1C and 2C spectra are not unexpected. The Wigner-sampled 1C spectrum of **1-Os** is very similar to that of **1-Ru**, with a broad and weak band in the 600 – 800 nm region, and a band splitting at ∼510 nm. The effect of Wigner sampling on the 2C spectrum of **1-Os** is relatively subtle with respect to the SP 2C. The low energy feature extends into the NIR and gains in intensity, leading to an improved agreement with the low-energy band observed experimentally. A second band just below 700 nm gains in intensity and matches a weak feature of the experimental spectrum between 650 – 700 nm. The band shape and intensity in the 550 – 650 nm region of the Wigner-sampled 2C spectrum also shows improved agreement with the experiment compared to the single-point spectrum. Only a limited number of transition energies could be included in the 2C calculations due to the computational cost associated with such simulations, and thus comparison with the experimental spectrum is not possible at wavelengths shorter than 550 nm. Overall, the Wigner-sampled 2C spectrum of **1-Os** is in better agreement with the experimental spectrum than the SP one, in the simulated range. Our observations suggest that it is predominantly spin-orbit coupling that leads to the appearance of the large band at 770 nm, as well as the shoulder observed at around 670 nm. However, the non-Condon effects do play a role by broadening the bands and altering the relative intensity of these two low-energy bands (compare the **1-Os** WIG 2C in Fig. 5 with **1-Os** SP 2C in Fig. 4).

In summary, the inclusion of non-Condon and SOC effects in the theoretical description of **1-Os** and **1-Ru** electronic excitations leads to a more accurate description of the shape of the absorption spectrum in its low-energy region, where electronic states all share a similar (MLCT) character. However, the high-energy region appears to be more challenging for LR-TDDFT/PBE0, already when switching on the effect of SOC for **1-Os** and as observed in earlier works on different osmium complexes.[31,60] Adding to the fact that the absolute energy of the different bands in the calculated spectrum appears to be in better agreement with experiment for **1-Os** than for **1-Ru**, although the electronic states in both systems appears to be very similar (*vide supra*), these two molecules may provide a compelling test case for further investigations of electronic-structure methods to reproduce excitation energies in large metal complexes. While the protocol described in this work is general, it is important to realize that it heavily relies on a proper description of the underlying electronic structure of the system.

Conclusion

In this work, we presented an investigation of the low-energy tail of the absorption spectrum of **1-Ru**, a Ru-based homoleptic biscyclometalated complex, by using advanced theoretical approaches combining relativistic LR-TDDFT calculations and the nuclear ensemble approach, as well as the synthesis and spectroscopic characterization of an analogous Os complex. The theoretical approach proposed in this work allows for the explanation of the absorption spectrum in terms of relativistic and non-Condon effects. We observed that, for **1-Ru** non-Condon effects and spin-orbit coupling lead to a similar broadening of the low-energy tail of the absorption spectra. Conversely, the role played by the much stronger spin-orbit coupling effect **1-Os** dominates over the non-Condon effects, even if the inclusion of the latter allows for a more precise reproduction of the experimental spectrum. Overall, the combination of spin-orbit coupling and non-Condon effects (via the nuclear ensemble approach) leads to an improved description of the shape of the low-energy tail of the absorption spectra for **1-Ru** and **1-Os**. More generally, this work shows that recent theoretical and computational developments make the inclusion of both spin-orbit and non-Condon effects possible in the simulation of absorption spectra for metal complexes with more than 100 atoms, even if such a protocol heavily relies on the quality of the underlying electronic-structure method. The methodology introduced here can be extended to the investigation of emission spectra, and work in this direction is currently in progress.

Conflicts of interest

There are no conflicts of interest to declare.

References

1 A. DeFusco, N. Minezawa, L. V. Slipchenko, F. Zahariev and M. S. Gordon, *J. Phys. Chem. Lett.*, 2011, **2**, 2184–2192.

2 B. Mennucci, *Int. J. Quantum Chem.*, 2015, **115**, 1202–1208.

3 T. J. Zuehlsdorff and C. M. Isborn, *Int. J. Quantum Chem.*, 2018, e25719.

4 E. J. Heller, *Acc. Chem. Res.*, 1981, **14**, 368–375.

5 A. Patoz, T. Begusic and J. Vanicek, *J. Phys. Chem. Lett.*, 2018, **9**, 2367–2372.

6 V. Barone, J. Bloino, M. Biczysko and F. Santoro, *J. Chem. Theory Comput.*, 2009, **5**, 540–554.

7 T. Sharp and H. Rosenstock, *J. Chem. Phys.*, 1964, **41**, 3453–3463.

8 W. Domcke, L. Cederbaum, H. Köppel and W. Von Niessen, *Mol. Phys.*, 1977, **34**, 1759–1770.

9 F. Santoro and D. Jacquemin, *Wiley Interdiscip. Rev. Comput. Mol. Sci.*, 2016, **6**, 460–486.

10 M. Barbatti, A. J. Aquino and H. Lischka, *Phys. Chem. Chem. Phys.*, 2010, **12**, 4959–4967.

11 R. Crespo-Otero and M. Barbatti, *Theor. Chem. Acc.*, 2012, **131**, 1237.

12 R. Crespo-Otero and M. Barbatti, *Chem. Rev.*, 2018, **118**, 7026–7068.

13 M. Barbatti and K. Sen, *Int. J. Quantum Chem.*, 2016, **116**, 762–771.

14 M. Ončák, L. Šištík and P. Slavíček, *J. Chem. Phys.*, 2010, **133**, 174303.

15 J. Suchan, D. Hollas, B. F. E. Curchod and P. Slavíček, *Farad. Discuss.*, 2018, **212**, 307–330.

16 M. Persico and G. Granucci, *Theor. Chem. Acc.*, 2014, **133**, 1–28.

17 R. Crespo-Otero and M. Barbatti, *J. Chem. Phys.*, 2011, **134**, 164305.

18 S. Mai, H. Gattuso, A. Monari and L. González, *Front. Chem.*, 2018, **6**, 495.

19 K. A. Phillips, T. M. Stonelake, K. Chen, Y. Hou, J. Zhao, S. J. Coles, P. N. Horton, S. J. Keane, E. C. Stokes, I. A. Fallis, A. J. Hallet, S. P. O'Kell, J. M. Beames and S. J. A. Pope, *Chem. Eur. J.*, 2018, **24**, 8577–8588.

20 L. González, D. Escudero and L. Serrano-Andrés, *ChemPhysChem*, 2012, **13**, 28–51.

21 E. Runge and E. K. U. Gross, *Phys. Rev. Lett.*, 1984, **52**, 997–1000.

22 M. E. Casida, *Recent Advances in Density Functional Methods*, Singapore, World Scientific, 1995, p. 155.

23 M. Petersilka, U. J. Gossmann and E. K. U. Gross, *Phys. Rev. Lett.*, 1996, **76**, 1212–1215.

24 C. A. Ullrich, *Time-Dependent Density-Functional Theory*, Oxford University Press, 2012.

25 F. Wang, T. Ziegler, E. van Lenthe, S. van Gisbergen and E. J. Baerends, *J. Chem. Phys.*, 2005, **122**, 204103.

26 F. Wang and T. Ziegler, *J. Chem. Phys.*, 2005, **123**, 154102.

27 M. Kühn and F. Weigend, *J. Chem. Theory Comput.*, 2013, **9**, 5341–5348.

28 A. R. Smith, P. L. Burn and B. J. Powell, *ChemPhysChem*, 2011, **12**, 2429–2438.

29 E. Baranoff, B. F. E. Curchod, F. Monti, F. Steimer, G. Accorsi, I. Tavernelli, U. Rothlisberger, R. Scopelliti, M. Grätzel and M. K. Nazeeruddin, *Inorg. Chem.*, 2011, **51**, 799–811.

30 J. M. Younker and K. D. Dobbs, *J. Phys. Chem. C*, 2013, **117**, 25714–25723.

31 E. Ronca, F. De Angelis and S. Fantacci, *J. Phys. Chem. C*, 2014, **118**, 17067–17078.

32 S. Fantacci, E. Ronca and F. De Angelis, *J. Phys. Chem. Lett.*, 2014, **5**, 375–380.

33 T. W. Rees, J. Liao, A. Sinopoli, L. Male, G. Calogero, B. F. E. Curchod and E. Baranoff, *Inorg. Chem.*, 2017, **56**, 9903–9912.

34 M. J. Frisch, G. W. Trucks, H. B. Schlegel, G. E. Scuseria, M. A. Robb, J. R. Cheeseman, G. Scalmani, V. Barone, B. Mennucci, G. A. Petersson, H. Nakatsuji, M. Caricato, X. Li, H. P. Hratchian, A. F. Izmaylov, J. Bloino, G. Zheng, J. L. Sonnenberg, M. Hada, M. Ehara, K. Toyota, R. Fukuda, J. Hasegawa, M. Ishida, T. Nakajima, Y. Honda, O. Kitao, H. Nakai, T. Vreven, J. A. Montgomery, Jr., J. E. Peralta, F. Ogliaro, M. J. Bearpark, J. J. Heyd, E. Brothers, K. N. Kudin, V. N. Staroverov, R. Kobayashi, J. Normand, K. Raghavachari, A. Rendell, J. C. Burant, S. S. Iyengar, J. Tomasi, M. Cossi, N. Rega, J. M. Millam, M. Klene, J. E. Knox, J. B. Cross,

V. Bakken, C. Adamo, J. Jaramillo, R. Gomperts, R. E. Stratmann, O. Yazyev, A. J. Austin, R. Cammi, C. Pomelli, J. W. Ochterski, R. L. Martin, K. Morokuma, V. G. Zakrzewski, G. A. Voth, P. Salvador, J. J. Dannenberg, S. Dapprich, A. D. Daniels, Ö. Farkas, J. B. Foresman, J. V. Ortiz, J. Cioslowski and D. J. Fox, *Gaussian 09, Revision D.01*, 2013.

35 C. Adamo and V. Barone, *J. Chem. Phys.*, 1999, **110**, 6158–6170.

36 F. Weigend and R. Ahlrichs, *Phys. Chem. Chem. Phys.*, 2005, **7**, 3297–3305.

37 D. Figgen, K. A. Peterson, M. Dolg and H. Stoll, *J. Chem. Phys.*, 2009, **130**, 164108.

38 F. Weigend and A. Baldes, *J. Chem. Phys.*, 2010, **133**, 174102.

39 E. R. Johnson and A. D. Becke, *J. Chem. Phys.*, 2006, **124**, 174104.

40 S. Grimme, J. Antony, S. Ehrlich and H. Krieg, *J. Chem. Phys.*, 2010, **132**, 154104.

41 S. Grimme, S. Ehrlich and L. Goerigk, *J. Comput. Chem.*, 2011, **32**, 1456–1465.

42 A. Klamt, C. Moya and J. Palomar, *J. Chem. Theory Comput.*, 2015, **11**, 4220–4225.

43 M. Barbatti, M. Ruckenbauer, F. Plasser, J. Pittner, G. Granucci, M. Persico and H. Lischka, *Wiley Interdiscip. Rev. Comput. Mol. Sci.*, 2014, **4**, 26–33.

44 D. Escudero and L. González, *J. Chem. Theory Comput.*, 2011, **8**, 203–213.

45 T. A. Niehaus, T. Hofbeck and H. Yersin, *RSC Advances*, 2015, **5**, 63318–63329.

46 T. Le Bahers, E. Brémond, I. Ciofini and C. Adamo, *Phys. Chem. Chem. Phys.*, 2014, **16**, 14435–14444.

47 D. Escudero and W. Thiel, *J. Chem. Phys.*, 2014, **140**, 194105.

48 D. Escudero and D. Jacquemin, *Dalton Transactions*, 2015, **44**, 8346–8355.

49 K. Kornobis, N. Kumar, B. M. Wong, P. Lodowski, M. Jaworska, T. Andruniów, K. Ruud and P. M. Kozlowski, *J. Phys. Chem. A*, 2011, **115**, 1280–1292.

50 K. Kornobis, N. Kumar, P. Lodowski, M. Jaworska, P. Piecuch, J. J. Lutz, B. M. Wong and P. M. Kozlowski, *J. Comput. Chem.*, 2013, **34**, 987–1004.

51 M. K. Armbruster, F. Weigend, C. van Wüllen and W. Klopper, *Phys. Chem. Chem. Phys.*, 2008, **10**, 1748–1756.

52 D. Peng, N. Middendorf, F. Weigend and M. Reiher, *J. Chem. Phys.*, 2013, **138**, 184105.

53 *TURBOMOLE V7.3 2018, a development of University of Karlsruhe and Forschungszentrum Karlsruhe GmbH, 1989-2007, TURBOMOLE GmbH, since 2007; available from http://www.turbomole.com*.

54 P. Pollak and F. Weigend, *J. Chem. Theory Comput.*, 2017, **13**, 3696–3705.

55 M. Kühn and F. Weigend, *J. Chem. Phys.*, 2015, **142**, 034116.

56 M. J. Peach, M. J. Williamson and D. J. Tozer, *J. Chem. Theory Comput.*, 2011, **7**, 3578–3585.

57 F. Plasser and H. Lischka, *J. Chem. Theory Comput.*, 2012, **8**, 2777–2789.

58 F. Plasser, *"TheoDORE 1.7: a package for theoretical density, orbital relaxation and exciton analysis"; available from http://theodore-qc.sourceforge.net*.

59 S. Tretiak and S. Mukamel, *Chem. Rev.*, 2002, **102**, 3171–3212.

60 S. Xu, J. E. Smith, S. Gozem, A. I. Krylov and J. M. Weber, *Inorg. Chem.*, 2017, **56**, 7029–7037.